Fire Safety Journal 152 (2025) 104347

Contents lists available at ScienceDirect

Fire Safety Journal

journal homepage: www.elsevier.com/locate/firesaf

Assessing the effect of oxidizer on flame geometry and effluent composition from burning solids

Jonathan Reep [a,*], José L. Torero [b], Rory M. Hadden [a]

[a] The University of Edinburgh, School of Engineering, Scotland, UK
[b] University College London, Faculty of Engineering Science, England, UK

ARTICLE INFO

Keywords:
Pyrolysis
Burning rate
Flammability
Emissions
Flame shape
PMMA
POM
FPA

ABSTRACT

The combustion chemistry and geometry of a diffusion flame are dictated by the transport of a fuel and an oxidizer towards a flame sheet. To enable the independent assessment of the impact of an oxidizer on a diffusion flame, the fuel injection rate must be controlled independently of the airflow. Through the independent control over the burning rate of the synthetic polymers polymethylmethacrylate (PMMA) and polyoxymethylene (POM), it is demonstrated that flame geometry can be systematically varied as a function of the oxygen environment. Both polymers were studied in the Fire Propagation Apparatus using a constant mass loss rate (MLR) under varying oxidative environments (177 L min^{-1}, 0 – 20.9 % vol O_2). This study draws upon frameworks developed for co-flow burners, allowing the characteristics of a diffusion flame to be established as a function of the oxidative environment. Flames sustained under lower oxidative environments displayed decreased luminosity and anchoring, with the heat flux from the POM flame decreasing by 14.7 kW m^{-2} as the oxygen concentration decreased from 20.9 % to 9.25 %. By relating combustion emissions to the flame geometry, through the use of a constant MLR, the processes controlling the emissions from the burning of solids have been studied in a novel manner.

1. Introduction

Understanding the composition of fire effluent enables insights into the solid and gas-phase processes of burning. For gaseous fuels, fire effluent is typically studied using experimental arrangements where the flows of both a fuel and an oxidizer can be independently controlled, e.g., in a co-flow burner. However, when studying combustible solids, the pyrolysis rate controls the gaseous fuel flow rate. The pyrolysis rate is determined by the surface energy balance which includes external heat fluxes and any heat feedback provided by the flame. The combination of these effects results in a strong coupling between the fuel flow rate and the oxidizer. To study the impact of the oxidizer to fuel ratio on the burning of solid fuels, it is therefore necessary to be able to independently control the pyrolysis rate.

1.1. Parameters controlling combustion chemistry in fires

In fires, combustible gases are generated when a condensed fuel gasifies (pyrolyzes) due to heat transfer from the flames and the surrounding environment. These combustible gases are transported by buoyancy effects and entrain air, supplying the oxygen necessary for combustion. As the fire increases in size, the characteristic flow velocity also increases, eventually transitioning to turbulence. It is the combination of these factors, the heat feedback, buoyancy and the turbulence, that controls the transport of both the fuel and the oxidizer towards the flame. These coupled phenomena ultimately establish the location of the flame and the characteristics of the combustion chemistry.

Within the flame itself, combustion chemistry can range from stoichiometric combustion, requiring conditions approaching the flame sheet approximation (i.e., infinitely fast chemistry), to quenching. As the flame approaches quenching, combustion chemistry is far from stoichiometric and is highly incomplete [1]. The fundamental principles describing the structure of diffusion flames have been studied for laminar flames arising from gaseous fuels [2]. However, this has not been translated to burning of solid fuels and turbulent flows which are relevant to fires.

1.2. Diffusion flame geometry

Laminar diffusion or non-premixed flames appear at the interface

* Corresponding author.
E-mail addresses: J.Reep@sms.ed.ac.uk (J. Reep), J.Torero@ucl.ac.uk (J.L. Torero).

https://doi.org/10.1016/j.firesaf.2025.104347
Received 16 July 2024; Received in revised form 20 January 2025; Accepted 21 January 2025
Available online 22 January 2025

between a stream of gaseous fuel and an oxidizer. The shape of these flames is defined by the region in which the fuel and oxidizer are consumed by the combustion reactions. The geometry of laminar diffusion flames arising from a gaseous fuel and an oxidizer has been described in detail by the Burke-Schumann development [3]. This development proposed that beyond the thin flame envelope, fuel and oxidizer cannot coexist, thus, combustion reactions are assumed to occur instantaneously. Burke and Schumann suggested that diffusion between the gaseous fuel and air within a coflow burner was the dominant contributor to flame geometry; greater than any contribution from velocity differences between the streams [4]. Following this work, flame shapes have been predicted with a remarkable degree of accuracy utilizing the Burke-Schumann development, aligning well with experimental results [5]. The size and geometry of the resultant laminar diffusion flame is therefore influenced primarily by the co-diffusion of fuel and oxygen towards the flame, alongside the oxidizer to fuel ratio.

An overventilated Burke-Schumann flame has a closed flame envelope generating primarily carbon dioxide (CO_2) and water vapor (H_2O), aligning with complete combustion. Under-ventilated conditions cause the flame to fan-out towards the oxidizer stream, creating a tulip shape that enables unburnt gases to escape through its center [6]. Despite these advances, the assumption that the flame will exist when the fuel and the oxidizer are delivered in stoichiometric proportions became a condition for determining the flame shape. Later studies using counterflow burners demonstrated that this is not always the case, with variables such a scalar dissipation having a significant role on the characteristics and location of the flame [7].

As the majority of fuels involved in fire scenarios begin in the condensed phase, the injection rate of fuel (the generation of pyrolysis gases) is controlled by the pyrolysis rate. This rate varies as a function of the combustion environment incorporating the effects of any external heating. As a result, the fuel injection rate becomes highly coupled to the external environment, where simplified configurations, such as those found in counter-flow burners, no longer enable interrogation of all the relevant variables. Assuming a one-dimensional heat balance, the mass loss rate (MLR) of the fuel can be approximated by the pyrolysis rate and under conditions of complete combustion, when the flame tip is closed, this is equal to the burning rate. Under-ventilated conditions will allow a fraction of the pyrolyzed gases to escape through the flame, under these conditions the MLR is not equal to the burning rate. As the MLR of a fuel will vary as a function of the oxidative environment, the impact of oxygen on flame geometry can only be assessed if the MLR remains fixed under a range of oxidative conditions that alter the flame geometry and the characteristics of the combustion chemistry.

1.3. Experimental configurations used to characterize the effluent from fire flames

Most previous studies on the characterization of effluent from fire-related flames have been conducted using the Cone Calorimeter (CC), the Fire Propagation Apparatus (FPA), the Steady State Tube (Purser) Furnace (SSTF) or the Micro Combustion Calorimeter (MCC) e.g., references [8–10]. These studies have established the variable nature of effluent composition but are all limited by the standard testing methodology. In the case of the MCC, pyrolysis products are mixed with oxidizer downstream of the solid sample resulting in the establishment of premixed flame. For the SSTF, the movement of oxygen towards the burning fuel results in a complex flow structure that is further influenced by secondary air in the mixing chamber. As a result, the combustion chemistry resembles an undefined combination of pre-mixed and non-premixed combustion. Computational fluid dynamics studies have shown that the characteristics of the flow remain in conditions where dissipation rates are negligible [11,12]. Flame geometry and quenching remain undefined and therefore the ratio between pyrolysis and combustion products cannot be related to the burning conditions. For other bench-scale studies, including CC and FPA studies, the burning rate is strongly coupled to the combustion environment, and it is not possible to decouple the thermal and species environments.

For the common diffusion-controlled flame, it is the flow of oxidizer in relation to the pyrolysis rate that dictates the overall flame geometry and hence the composition of the effluent. The qualitative flame shape enables an insight into the transport rate of oxidizer into the flame sheet. As the oxygen diffusing towards the flame controls the combustion processes, the oxidizer composition may be varied in order to screen a range of flame geometries. However, changing the airflow induces changes in the burning rate, altering the combustion processes. Quenching may be determined based upon a disappearance of a visible flame luminosity. To successfully observe the effects of varying the oxygen reaching the flame, the MLR needs to be fixed, and independently controlled, enabling the impact of the oxidizer flow on flame geometry to be independently assessed.

For the flame geometry to be fixed, the geometry of the experimental set-up and the velocity of the fuel and oxidizer need to be independently controlled. To achieve this, a controllable external heat flux must be implemented, that can deliver an appropriate time dependent heat flux to the solid such that pyrolysis occurs at a constant rate. Once a constant pyrolysis rate has been established, the air flow can be controlled and the effects on the flame observed (e.g., geometry, luminosity). The analysis of the chemical species being generated may be used to determine the extent of the pyrolysis and whether secondary oxidative processes are occurring [13]. Furthermore, monitoring carbon monoxide (CO) and CO_2 enables the completeness of any combustion to be assessed. Such an approach allows for the detailed exploration of the evolution of the pyrolysis and combustion products whilst considering the flame geometry as an intrinsic characteristic of all diffusion flames. It is the combination of the flame geometry and the emissions data that is used to characterize the burning. The link between these two parameters enables the source of pyrolysis gases to be determined, whether that be due to changes in the flame geometry or local/global extinction.

Whilst the FPA can control the heat flux and flow variables independently, there are some limitations that mean direct comparison to the Burke-Schumann framework is not possible. These primarily arise due to the flow conditions around the pyrolyzing sample including the effects of the bluff body, buoyancy and turbulence. Therefore, in this work, we seek to apply the ideas of the theory rather than obtain direct comparisons.

1.4. Polymer flammability

The MLR during combustion is governed by Equation (1). The MLR is dependent on the net heat flux at the surface of a sample including contributions from: the external heating $(\dot{Q}_E^{''})$, the flame $(\dot{Q}_F^{''})$, heat losses from the surface $(\dot{Q}_L^{''})$, and the heat of vaporization (pyrolysis) (L_v) of the solid [14,15]. Usually, during fire testing a constant $\dot{Q}_E^{''}$ is used and $\dot{Q}_F^{''}$ and $\dot{Q}_L^{''}$ will evolve depending on the material properties and the flame dynamics. Changing $\dot{Q}_E^{''}$ in time compensates for time dependent behavior if $\dot{Q}_F^{''}$ and $\dot{Q}_L^{''}$ deliver a constant net heat flux to the surface; resulting in a constant pyrolysis rate.

$$MLR = \frac{\dot{Q}_E^{''} + \dot{Q}_F^{''} - \dot{Q}_L^{''}}{L_v} \tag{1}$$

A true steady state combustion process involves control over the MLR and has been demonstrated to be effective as a novel means of assessing pyrolysis products [13,16]. A steady state MLR can be achieved by measuring the real-time MLR and using a proportional integral derivative (PID) controller to vary the heat flux provided by the FPA heat lamps (i.e., manipulating $\dot{Q}_E^{''}$). Varying the oxygen concentration whilst maintaining a fixed burning rate enables the transition from combustion to pyrolysis to be probed in a more systematic manner, providing insight

into the changing magnitude of $\dot{Q}_F^{''}$.

By making the MLR a fixed control variable, both the supply of gaseous fuel (pyrolyzate) and the composition of the oxidizer stream can be independently controlled. This control enables flame geometry to be explored alongside the composition of the effluent and the identification of flame quenching behavior as a function of the combustion environment.

2. Methods and materials

2.1. Materials

Polyoxymethylene (POM) - type h (homopolymer) and polymethylmethacrylate (PMMA) were commercially sourced. These opaque, black samples were cut into spherical discs with a 70 mm diameter. The influence of oxygen supply on the burning of these material using the FPA has been previously examined in literature [17]. Due to the greater ideal burning rate for PMMA compared to POM, thicker samples, 21 mm, were required to obtain a similar combustion duration to the POM, 12 mm [18]. These samples weighed 100 g (PMMA) and 75 g (POM) respectively. The rear faces of each polymer were wrapped in foil to prevent molten material falling from the sample holder.

POM is a polyacetal thermoplastic, resulting in a structure with a high percentage of oxygen by mass. This abundance of oxygen results in POM burning with an essentially soot-free, non-luminous (blue) flame [19]. Although oxygen is also present within the structure of PMMA, the ratio of oxygen to hydrogen and carbon is significantly reduced, thus, PMMA burns with luminous diffusion flame, resulting in increased radiative energy losses from the system. When these polymers are exposed to an external heat flux, pyrolysis will occur principally generating their respective monomers; formaldehyde (CH_2O) and methyl methacrylate (MMA, $C_5H_8O_2$). Both POM and PMMA have been reported to exceed ≥90 % monomer recovery during pyrolysis [20–23].

During flaming combustion, the pyrolysis products generated pass through the flame envelope and are oxidized to produce a variety of combustion products including CO, CO_2 and H_2O. In the event that adequate ventilation is unavailable, incomplete oxidation of MMA and formaldehyde will occur. Under such scenarios formaldehyde has been shown to generate CO, as outlined by Equation (2) [23].

$$CH_2O \rightarrow CO + H_2 \quad (2)$$

Such an equation implies that CO generation from formaldehyde is possible under completely inert conditions.

2.2. Methodology

2.2.1. The burning rate

Samples were required to burn, or pyrolyze, for an extended period, 1400 s, to generate a stabilized flame for effluent sampling. Given the high flow rate of the oxidizer stream, 177 L min^{-1}, a high burning rate was selected for each polymer to ensure combustion species and pyrolysis gases were being generated above the limits of detection. Burning rates of 5 g s^{-1} m^{-2} and 13 g s^{-1} m^{-2} were selected for POM and PMMA respectively, based on analysis in preliminary trials.

2.2.2. Steady state control

Samples of each polymer were placed onto a pedestal connected to a load cell situated within the combustion chamber of the FPA. A quartz tube (435 mm high, outer diameter 174 mm, inner diameter 164 mm) was placed over the sample. A pilot flame (60 % air, 40 % ethylene) was present during each trial, facilitating ignition. Once ignited, this pilot flame was switched off.

The FPA lamps were controlled by a PID controller to achieve a constant MLR using the method described in Reep et al., alongside the addition of a pilot flame and a stationary camera with a fixed ISO [13]. The PID controller worked on a feedback loop where the output voltage being sent to the FPA lamps was dictated based upon the difference between the real-time and the target MLR values. The proportional, integral and derivative constants of the PID controller were set to $K_p = 2$, $K_i = 0.01$, and $K_d = 8$, respectively.

After an initial ramp (0.02 kW m^{-2} s^{-1}, 60 s) the PID controller was initiated, controlling the voltage supplied to the lamps and therefore the heat flux supplied to the specimen. Constant mass loss rates of 5 g s^{-1} for the POM and 13 g s^{-1} for the PMMA were set over the 1400 s time period.

Once ignited by the pilot, samples were allowed to stabilise in air for 200 s prior to the intended oxidative environment being introduced. The oxidative environment was gradually adjusted over 500 s minimising disturbance to the flame. Once the intended oxidative environment had stabilized, 200 s, sampling commenced (t = 900 s), with emission sampling occurring for 500 s from this point. The composition of the oxidiser stream was set to each of the oxygen percentages outlined in Table 1, with the balance being nitrogen.

Based upon preliminary trials, oxidative conditions were chosen to encompass the region in which flaming combustion quenched and the sample behavior transitioned to pyrolysis only; ~9.25 % and ~12.75 % O_2 for POM and PMMA, respectively. Oxygen concentrations were selected either side of these values to incorporate those which readily sustained a flame and those in which only pyrolysis was expected to occur.

In addition to the experiments at constant oxidative environments, experiments were also conducted in which the oxidative environment was changed from 20.9 % to 0 % oxygen. In these cases, after the PID controller was initiated and ignition was achieved, the sample was allowed to stabilise under 20.9 % oxygen until 400 s had elapsed. Beyond this point, the oxygen concentration was decreased to each value listed in Table 1 every 150 s.

2.2.3. Exhaust gas sampling

For every trial, effluent was sampled above the quartz tube (150 mm) via a heated sampling line (453 K) passing into a Fourier-transform infrared spectroscopy (FT-IR) cell (Gasmet, Vantaa, Finland), with a reading occurring every 3 s. FT-IR analysis was conducted using a Gasmet DX4000 portable gas analyser. Produced IR spectra were analysed using the supplied software (Calcmet V2005.100, Tetmet Instruments Ltd., Vantaa Finland) alongside calibrated reference spectra (20, 51, 700 and 1000 ppm for MMA and 24.9, 45.6, 78.3 and 136.9 ppm for formaldehyde). Each spectrum was analysed across a spectral range (595–4240 cm^{-1}) with the resolution (4 cm^{-1}) achieved via a thermo-electrically cooled MCT detector coupled with an antireflection (ZnSe) beamsplitter. Gas samples were filtered (particulate, 2 μm) before entering the sample cell (0.4 L, 453 K). The path length (250 cm) proved adequate to maintain the sampling frequency.

The following absorption bands were used to identify the monomers

Table 1
The average (mean) and standard deviation (SD) of the smoothed mass loss rates (MLRs) for POM and PMMA over several differing atmospheres O_2/ % ±0.16.

POM			PMMA		
O_2/ %	MLR/ g s^{-1} m^{-2}	SD/	O_2/ %	MLR/ g s^{-1} m^{-2}	SD/
0	5.02	0.08	0	12.60	0.38
5	5.05	0.16	5	13.04	0.16
7	5.07	0.41	10	12.00	1.03
8.5	5.02	0.09	12.5	12.48	0.44
9	4.94	0.12	12.75	13.09	0.12
9.25	5.07	0.08	13	12.99	0.33
9.5	5.21	0.25	13.5	13.04	0.24
10	5.25	0.21	14	13.16	0.30
15	5.23	0.27	15	13.01	0.12
18	5.68	0.18	18	12.90	0.18
20.9	6.74	0.21	20.9	13.77	0.60

MMA, 1150, 1355 and 1750 cm^{-1} and formaldehyde, 1500, 1750 and 2850 cm^{-1}. Multiple bands were fitted in each of these ranges (±25 cm^{-1}) to positively identify and quantify the monomers.

3. Results

Fig. 1 displays the MLR values obtained for both the PMMA and the POM. The highest MLR values for each polymer were achieved under an ambient atmosphere (20.9 % O_2). Under these ambient conditions complete combustion readily occurred, increasing the heat feedback to the surface of the polymer. The values across the other investigated oxygen conditions were largely consistent, indicating that the MLR was adequately controlled by the PID controller during flaming combustion. Flames were quenched below 12.75 % and 9.25 % O_2 for PMMA and POM respectively, at which point the MLR was equal to the pyrolysis rate.

3.1. Qualitative flame geometries

Fig. 2 shows annotated still images of the flame shape obtained during the burning of PMMA under different oxidizer streams. Similar observations were made for POM. Images were selected from periods of low incident heat flux, as the light from the FPA lamps prevented visualization of the flame envelope during periods of higher incident heat flux. Although qualitative, these images can be used to describe the evolution of the flame shape across the investigated atmospheres.

Under the 20.9 % and 18.0 % O_2 environments the flame envelope appeared to completely close, indicating complete combustion, thus largely preventing the emission of unoxidized species. The higher oxygen concentrations resulted in the most luminous flame, as highlighted in Fig. 2. As the oxidative conditions decreased, FT-IR data showed an increased CO yield, indicating a lower combustion efficiency. Flame luminosity, and therefore combustion efficiency, was observed to decrease under lower oxidative environments.

As predicted by the Burke-Schumann development, flame heights varied with the oxidative environment. At lower oxygen concentrations, the reduced concentration gradient decreased the rate of oxygen diffusion to the flame which in turn decreased the reaction rate and flame temperature resulting in lower combustion efficiency. These lower flame temperatures consequently reduced the rate of oxygen diffusion to the flame front, resulting in an increase in the average flame height [24].

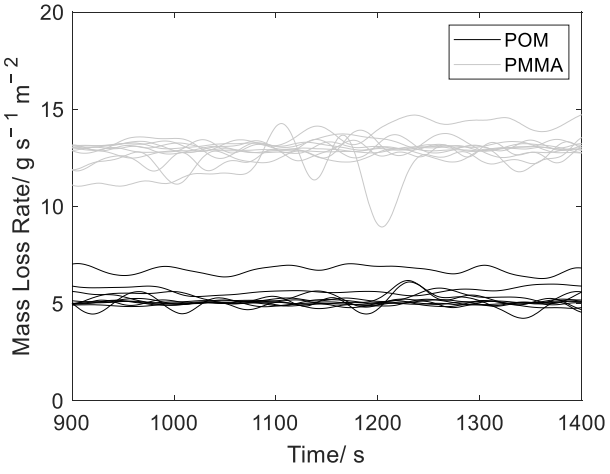

Fig. 1. The smoothed (Gaussian filter, 60 periods) mass loss rates (MLR) observed for PMMA and POM under each of the investigated oxygen environments. The MLR was successfully being controlled, regardless of the oxidative conditions. The greatest deviations from the set MLR occurred at 20.9 % O_2 for the POM and at 10 % O_2 for the PMMA.

Moving towards the lower oxidative environments displayed in Figs. 2 and 12.75 % and 13 % O_2, the flame tips are shown to have widened. It is plausible to suggest that species generated from the surface of the polymer were emitted into the effluent without interacting with the flame envelope. This is particularly evident at 12.75 % O_2 where the central 'passage' within the flame has opened up. The flame appears to have many of the characteristics of the Burke-Schumann flame structure albeit within a less well controlled environment. Quantitative measurements to support these observations can be made, and are discussed in the following sections.

3.2. Quantifying changes in flame geometry

A quantitative analysis of the average PMMA flame location (defined by a threshold intensity of the red channel in the video during periods where the FPA lamps did not result in image saturation) is presented in Fig. 3 for each of the investigated oxygen environments. This figure shows the flame location averaged over a 500 s window during the steady burning period when the image intensity was not dominated by the FPA lamps.

The asymmetric nature of the flame observed at 12.75 % O_2 is likely to have arisen as a result of cropping the video frames to block out the FPA lamps. At low oxygen concentrations, 12.75 % O_2, the flame region was on average located ~90 mm further away from the sample surface than under ambient oxidative environments. As the concentration of oxygen was increased, the flame anchored closer to the sample. This anchoring reduced the average flame height from ~225 mm to ~45 mm. The areas of red in Fig. 3, more prominent across a greater range of heights under the decreased oxidative environments, highlight the variability in the flame location, indicative of the flame structures formed during under-ventilated combustion.

The flames at higher oxidizer concentrations in Fig. 3 appeared to consist of two parts. The apparent upper part of the flame, observed at 18 % and 20.9 % O_2, is a reflection of the flame in the FPA quartz tube. A combination of the reduced flame heights and greater luminosities enhanced this reflective effect under these oxidative conditions. These reflections could not be easily removed during the image analysis, only becoming notable for short, luminous flames. Under higher oxygen environments the fuel flow rate became the limiting factor to determine flame height, thus shorter flames were observed as the fuel was oxidized closer to the surface of the polymer. Under reduced oxidative conditions, this oxidation happened much further from the polymer surface, resulting in increased flame lengths.

The heat flux delivered by the FPA lamps to maintain the constant MLR for each material as a function of the oxidative environment is presented in Fig. 4. A greater heat flux was required to sustain the same MLR under lower oxidative environments for both POM and PMMA. This trend was consistent between materials, with both polymers exhibiting an independence from the oxygen environment for concentrations greater than 18 % O_2. This heat flux trend indicated that less energy was being returned to the surface of the polymer by the flame.

A small increase in the heat flux required to sustain the MLR of POM was noted at lower oxidative conditions in the absence of flaming. This finding suggested that the pyrolysis of POM had more of an oxygen dependency than PMMA, however further investigation into these processes would be required before any conclusions can be drawn.

By reference to Equation (1), if the energy loss, $\dot{Q}''_L$, is assumed to be a constant for each material, 21.3 kJ g^{-1} and 13.8 kJ g^{-1} for PMMA and POM respectively, then rearrangement of Equation (1) enables the heat flux supplied by the flame to the sample's surface, $\dot{Q}''_F$, to be calculated [14,25]. Assuming L_v values of 1.62 kJ g^{-1} and 2.43 kJ g^{-1} for PMMA and POM respectively, the heat flux supplied by the flame for the POM and PMMA was calculated and is shown in Fig. 5.

Fig. 5 shows the heat feedback from the flame for the cases where flaming combustion occurred. Values below 9.25 % O_2 could not be

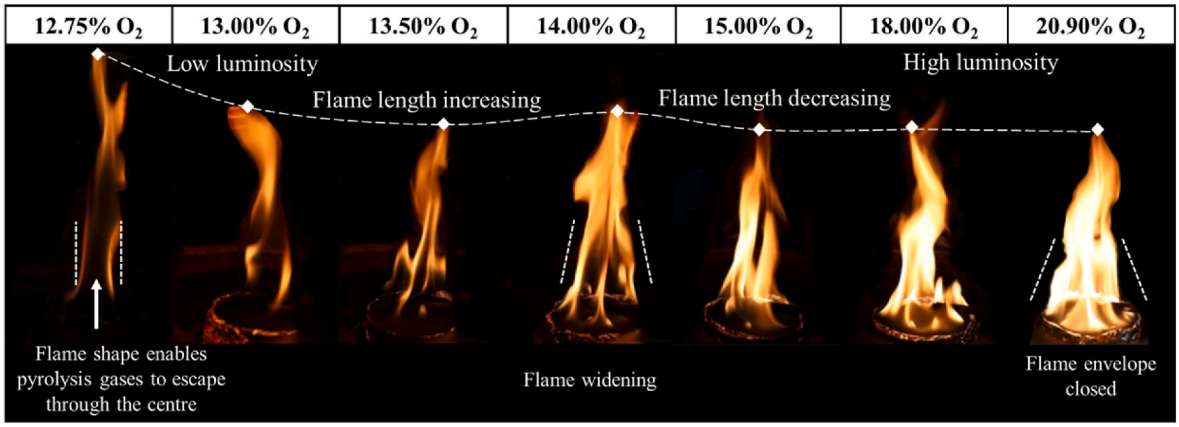

Fig. 2. The turbulent PMMA flames observed between 20.90 % and 12.75 % O_2. Individual video frames have been taken as the light from the FPA lamps prevented time averaging. Note the images, taken between 300 s and 450 s during an oscillation where the FPA lamps started to dim, have been edited to remove the background glare from the quartz tube.

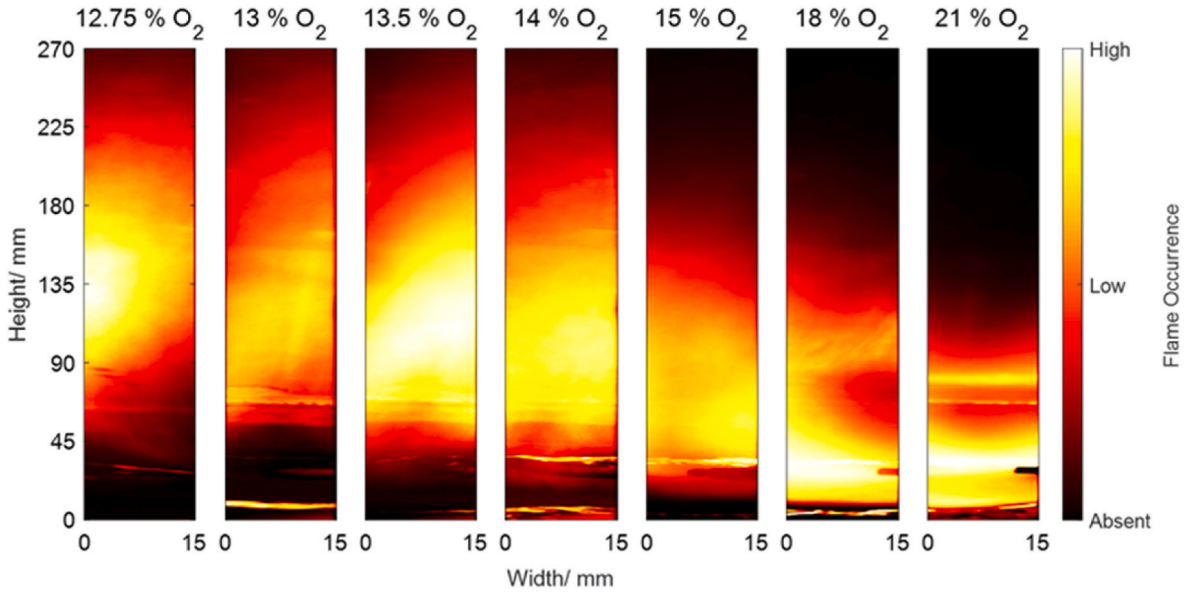

Fig. 3. The average flame location for the steady burning of PMMA taken over a 500 s window for each oxygen concentration. White/yellow indicates areas of high flame occurrence and black the absence of flame. Note that the images have been taken from a slight offset and that reflections of the flame in the quartz tube could not be removed from the analysis. (For interpretation of the references to colour in this figure legend, the reader is referred to the Web version of this article.)

obtained due to the absence of a flame. The heat feedback supplied by the flames for PMMA at 12.75 % O_2 and POM at 9.25 % O_2 were slightly greater than their neighboring values. Visual observations for these experiments confirmed the emission of pyrolysis gases through the flame, indicating the presence of an instability and the onset of flame quenching.

It is interesting to observe that despite the significant differences in the flame luminosity and shape, the average values of $\dot{Q}_F''$ for the POM and PMMA under a given oxygen environment are approximately equal. Linear fuels containing oxygen, like POM and PMMA are known to have similar $\dot{Q}_F''$ values [25]. The individual contributions to $\dot{Q}_F''$ from the flame temperature and the soot volume fraction could not be distinguished. It is likely that the PMMA flame had a lower flame temperature but a higher contribution from radiative transfer when compared to the soot-free POM flame. In this case, the combined impact of these differences resulted in very similar values of $\dot{Q}_F''$ being obtained. This is in agreement with existing literature where $\dot{Q}_F''$ values for both PMMA and POM are given as 38.5 kW m^{-2} [25]. The magnitude differs to the values reported here, 25.4 $\pm$ 2.2 kW m^{-2}, likely due to differing methodologies. Nevertheless, the similarity between the polymers within each study is noteworthy.

Between 9.25 % and 10 % O_2, POM sustained a weak flame. Visual similarities between these flames mirrored the clustering of the calculated $\dot{Q}_F''$ values around 11 kW m^{-2}. As with the PMMA, the slight rise in heat flux supplied by the flame under the lowest oxidative conditions that sustained flaming, suggested the presence of instabilities around the flame quenching point. It therefore followed that the flaming combustion of POM occurred in a similar manner under low oxidative conditions, however, more intermediate oxygen percentages would enhance confidence in the data and firm up the apparent trends.

3.3. Effluent composition

The changes in flame shape and flame heat feedback suggested that the emissions would also vary as a function of the oxygen concentration as predicted by the Burke-Schumann framework. When sampling of fire effluent compromises must be made. Utilizing analytical techniques like

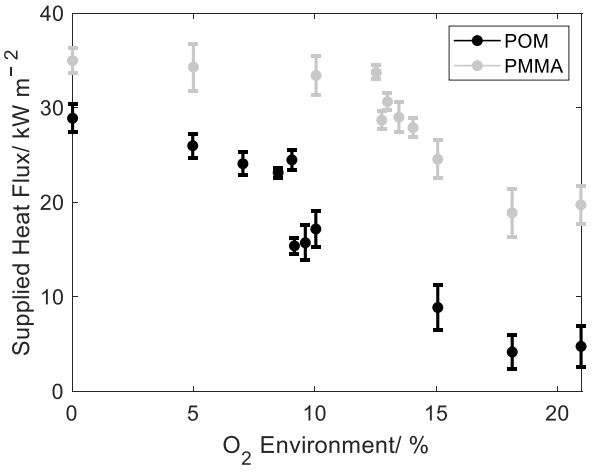

Fig. 4. The average heat flux required to maintain the set MLR for PMMA (13 g s^{-1} m^{-2}) and POM (5 g s^{-1} m^{-2}) over a range of oxidative environments.

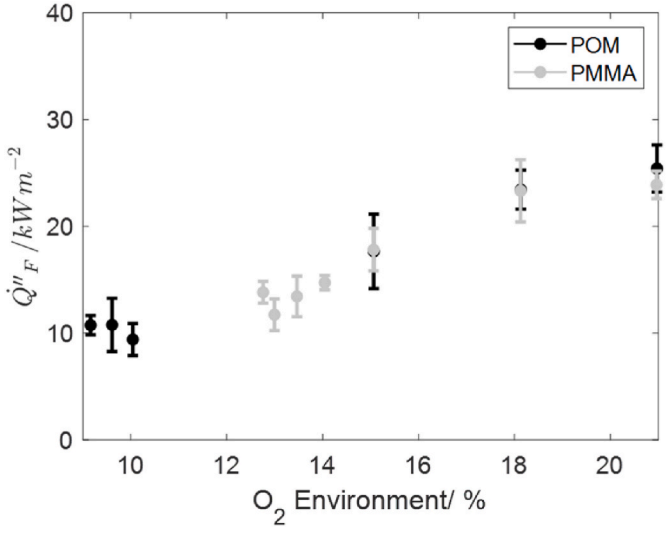

Fig. 5. The average heat feedback supplied by the flame for PMMA and POM over a range of oxidative environments across the six or seven oxidative conditions at which flaming combustion was sustained. These values have been calculated using latent heat of vaporization (L_v) and $\dot{Q}''_L$, values from literature [25].

FT-IR result in gases being measured at thermal and chemical equilibrium, however the noninvasive nature of the technique alongside the near real time readings have increased its prominence in the field. To mitigate differences in the exhaust stream flow rate, product yields (instead of concentrations) are presented.

After a 900 s stabilization period, sampling of CO_2, CO and the monomers (MMA and formaldehyde) commenced. Readings were made every 3 s, resulting in 165 points for each investigated condition; effectively 165 repeats. As such, an average value for the yields was calculated with error bars showing twice the standard deviation of each dataset. The magnitude of the error bars reflects both the error in the FT-IR measurement and the occasional intermittent generation of pyrolysis gases when the PID controller adjusted the MLR sample. The yields of the products obtained during PMMA and POM combustion are summarized in Figs. 6 and 7. The resolution of the FT-IR analysis, 4 cm^{-1}, is below the full width half maximum absorption transitions for formaldehyde, thus it is likely that a level of uncertainty was introduced when

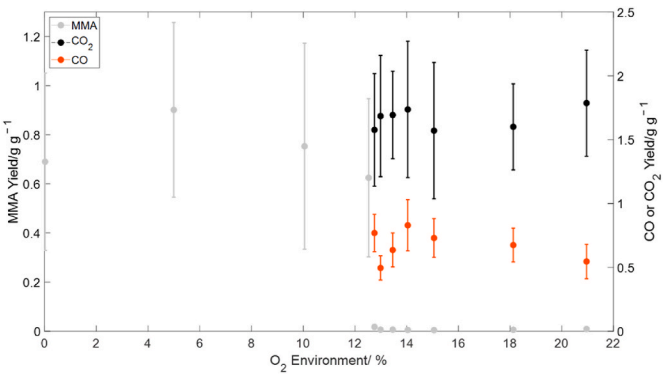

Fig. 6. The average yields of CO_2, CO and the monomer MMA from PMMA combustion across a range of oxidative conditions.

identifying this monomer, explaining the low yields. Under the conditions tested, flaming combustion could not be sustained below 12.75 % and 9.25 % O_2 for the PMMA and POM respectively. This resulted in pyrolysis and thus high monomer yields.

Fig. 6 shows that the yield of the monomer MMA at concentrations below 12.75 % O_2 was approximately 1 g g^{-1}; suggesting an absence of oxidative processes. There was some evidence of a potential decrease in the MMA yield as the oxygen concertation was increased, which may have arisen due to different oxygen-dependent pyrolysis pathways occurring, resulting in differing solid-phase decompositional processes. Additionally, the gas-phase oxidation of MMA into intermediate gaseous species may have been more favorable under higher oxidative conditions. A change in effluent composition was observed around the oxygen environments required to enable flaming combustion. Under these conditions, the monomer yield was significantly reduced however, MMA was still being generated alongside flaming combustion with a yield of 0.02 g g^{-1} recorded at 12.75 % O_2. These findings mimic the response of the "open" flame structure described in the Burke-Schumann framework; in which the flame envelope opens under low oxygen conditions, enabling pyrolysis gases to escape, albeit under conditions suspectable to buoyancy-induced effects. To assess this effect further, the combustion environment needed altering. Above 12.75 % O_2, the yield of monomer decreased to approximately zero and the yield of CO and CO_2 increased. The yield of CO_2 was approximately 1.7 g g^{-1} and the yield of CO varied between 0.7 and 0.5 g g^{-1} (decreasing as the O_2 concentration was increased).

The POM displayed similar trends in monomer production with the yield of monomer dropping to zero as flaming combustion was established (9.25 % O_2). The key difference between the polymer emissions, aside from the differing monomers, is found in the CO yields. For the POM, CO production aligned with pyrolysis with yields in the region of 0.2 g g^{-1}; presumably generated by the process described by Equation (2) [23]. The CO generated by Equation (2) gradually decreased as the oxidative conditions rose from 9.25 % to 10 % O_2 as the flame geometry started to limit the emission of unoxidized species. At higher oxidative environments, CO was fully oxidized, with CO_2 being detected as a combustion product. When flaming was present, CO_2 was generated at a constant yield of approximately 1.15 g g^{-1}. The yield of CO_2 was at approximately the stoichiometric limit suggesting effectively complete combustion when the oxygen concentration was above 10 % O_2.

The reverse observation was made when assessing the CO yield generated by the PMMA. CO was not generated in the absence of a flame, below 12.75 % O_2. Once a flame was established, the open flame geometry between 12.75 % and 15 % O_2 enabled partially oxidized species, like CO, to enter the effluent. As these values are fairly large and steady, it is plausible that some post combustion oxidation occurred after the effluent exited the quartz tube. Beyond 18 % O_2 the closed flame structure enabled a greater extent of oxidation causing the CO

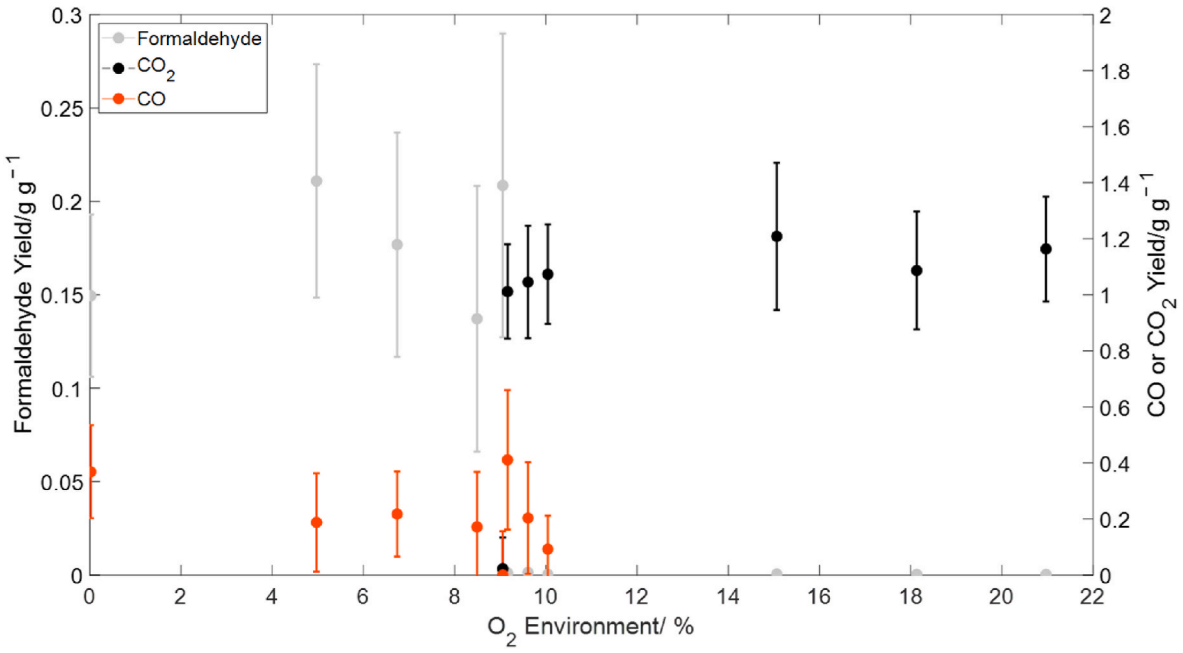

Fig. 7. The average yields of CO_2, CO and the monomer formaldehyde from POM combustion across a range of oxidative conditions.

yield to decrease.

3.4. The combustion environment

As both the monomer and CO_2 yields were shown to vary either side of the flaming combustion transition, both were expected to be recorded at intermediate levels across intermediate oxygen environments. However, as Fig. 8 shows, the transition between pyrolysis and flaming combustion resulted in a relatively sudden yield transition.

Sweeping the oxygen concentration over the quenching region, demonstrated that the ratio between pyrolysis and combustion products changed abruptly over a range of approximately 0.2 % O_2 between 12.41 % and 12.57 % O_2. Once the flame had begun to open up, and monomer yields rose slightly, the flame was rapidly quenched; resulting in effluent dominated by pyrolysis species.

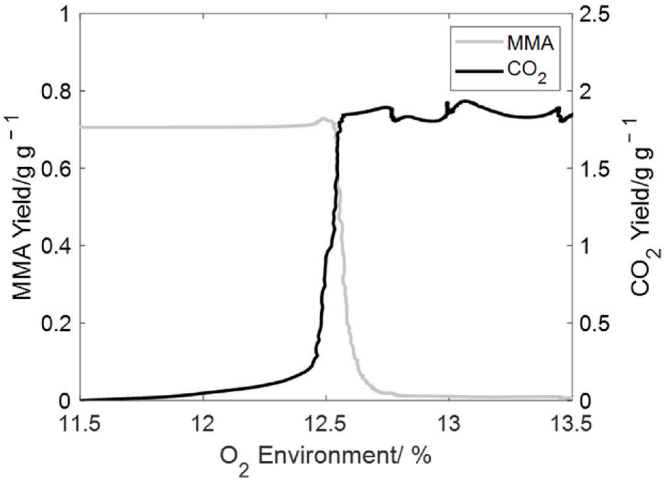

Fig. 8. The obtained yield of MMA and CO_2 during the combustion of PMMA between 11.5 % and 13.5 % O_2.

4. Conclusions

Through the independent control over the MLR of synthetic polymers, it is demonstrated that the flame geometry can be systematically varied. By fixing the MLR for POM and PMMA over a range of oxidative conditions, the impact of ventilation on diffusion flames can be decoupled from the burning rate, enabling the impact of oxidizer flow on flame geometry to be independently assessed. This work focused on coupling the solid phase processes (pyrolysis) with the gas phase processes (combustion), enhancing our understanding of the impact of flame geometry on effluent composition for condensed-phase fuels.

Visual observations, calculation of the flame heat feedback and measurement of the effluent, indicated behavior similar to that observed in the Burke-Schumann framework. The objective, to obtain flame geometries under differing oxidizer streams, could be further quantified through a greater resolution of the airflows within the FPA however, the intent was never to predict Burke-Schumann structures using the FPA. At oxygen concentrations greater than those required to sustain flaming combustion, flames were observed to be closed and effluent contained products of complete combustion. As the oxygen environment was decreased, flames widened and decreased in luminosity, enabling the emission of unoxidized pyrolysis species. $\dot{Q}''_F$ values dropped from 25.4 kW m^{-2} to 9.4 kW m^{-2} for POM and from 23.8 kW m^{-2} to 13.0 kW m^{-2} for PMMA, while CO_2 yields fell, relative to flaming combustion under ambient conditions, reflecting the decreased combustion efficiency of the flames.

This methodology can be used to evaluate the combustion effluent generated under varying oxygen conditions in diffusion flames. Extending the method to other materials will allow source terms to be generated for use with numerical tools to predict the rates of generation of combustion species.

CRediT authorship contribution statement

Jonathan Reep: Writing – original draft, Methodology, Investigation, Formal analysis. **José L. Torero:** Writing – review & editing, Supervision, Conceptualization. **Rory M. Hadden:** Writing – review & editing, Supervision, Conceptualization.

Declaration of competing interest

The authors declare that they have no known competing financial interests or personal relationships that could have appeared to influence the work reported in this paper.

Appendix A. Supplementary data

Supplementary data to this article can be found online at https://doi.org/10.1016/j.firesaf.2025.104347.

Data availability

Data will be made available on request.

References

[1] A. Liñán, The asymptotic structure of counterflow diffusion flames for large activation energies, Acta Astronaut. 1 (1974) 1007–1039, https://doi.org/10.1016/0094-5765(74)90066-6.

[2] F.A. Williams, Combustion Theory, second ed., CRC Press, 2018 https://doi.org/10.1201/9780429494055.

[3] S.P. Burke, T.E.W. Schumann, Diffusion flames, Ind. Eng. Chem. 20 (1928) 998–1004, https://doi.org/10.1021/ie50226a005.

[4] I. Glassman, R.A. Yetter, Combustion, fourth ed., Elsevier Inc., 2008.

[5] S. Fukutani, N. Kunioshi, H. Jinno, Flame structure of an axisymmetric hydrogen-air diffusion flame, Symposium (International) on Combustion 23 (1991) 567–573, https://doi.org/10.1016/S0082-0784(06)80304-8.

[6] C. Clanet, G. Searby, On the "tulip flame" phenomenon, Combust. Flame 105 (1996) 225–238, https://doi.org/10.1016/0010-2180(95)00195-6.

[7] I.K. Puri, K. Seshadri, Extinction of diffusion flames burning diluted methane and diluted propane in diluted air, Combust. Flame 65 (1986) 137–150, https://doi.org/10.1016/0010-2180(86)90015-5.

[8] A.A. Stec, T.R. Hull, K. Lebek, Characterisation of the steady state tube furnace (ISO TS 19700) for fire toxicity assessment, Polym. Degrad. Stabil. 93 (2008) 2058–2065, https://doi.org/10.1016/j.polymdegradstab.2008.02.020.

[9] R.N. Walters, N. Safronava, R.E. Lyon, A microscale combustion calorimeter study of gas phase combustion of polymers, Combust. Flame 162 (2015) 855–863, https://doi.org/10.1016/j.combustflame.2014.08.008.

[10] S. Brohez, G. Marlair, C. Delvosalle, Fire calorimetry relying on the use of the fire propagation apparatus. Part II: burning characteristics of selected chemical substances under fuel rich conditions, Fire Mater. 30 (2006) 35–50, https://doi.org/10.1002/fam.897.

[11] A. Mahalingam, F. Jia, Z. Wang, M.K. Patel, E.R. Galea, Numerical investigation of tube furnace toxicity measurement method (ISO 19700), Fire Mater. 36 (2012) 17–30, https://doi.org/10.1002/fam.1079.

[12] Z. Liu, H. He, Y. Chen, J. Zheng, H. Zhuang, Experimental investigation and numerical modelling of CO and HCN release during the combustion of flexible polyurethane foam, J. Anal. Appl. Pyrolysis 174 (2023) 106141, https://doi.org/10.1016/j.jaap.2023.106141.

[13] J. Reep, J.L. Torero, R.M. Hadden, An approach for the improved measurement of pyrolysis products, Fire Saf. J. 142 (2024) 104037, https://doi.org/10.1016/j.firesaf.2023.104037.

[14] D. Drysdale, An Introduction to Fire Dynamics: Third Edition, an Introduction to Fire Dynamics, Third Edition, 2011, pp. 1–551, https://doi.org/10.1002/9781119975465.

[15] I. Glassman, Comments on: flammability of plastics—I. Burning intensity by A. Tewarson and R.F. Pion, Combust. Flame 29 (1977) 103–105, https://doi.org/10.1016/0010-2180(77)90099-2.

[16] S. Santamaria Garcia, Ignition of solids exposed to transient irradiation. https://doi.org/10.7488/ERA/1708, 2021.

[17] A. Tewarson, J.L. Lee, R.F. Pion, The influence of oxygen concentration on fuel parameters for fire modeling, Symposium (International) on Combustion 18 (1981) 563–570, https://doi.org/10.1016/S0082-0784(81)80061-6.

[18] G.H. Markstein, Radiative properties of plastics fires, Symposium (International) on Combustion 17 (1979) 1053–1062, https://doi.org/10.1016/S0082-0784(79)80101-0.

[19] I.T. Leventon, K.T. Korver, S.I. Stoliarov, A generalized model of flame to surface heat feedback for laminar wall flames, Combust. Flame 179 (2017) 338–353, https://doi.org/10.1016/J.COMBUSTFLAME.2017.02.007.

[20] I.C. Sanders, N.M. Kuenning, N.Q. Minesi, D.I. Pineda, R.M. Spearrin, Methyl methacrylate thermal decomposition: modeling and laser spectroscopy of species time-histories behind reflected shock waves, Fuel 335 (2023) 126846, https://doi.org/10.1016/J.FUEL.2022.126846.

[21] W.R. Zeng, S.F. Li, W.K. Chow, Preliminary studies on burning behavior of polymethylmethacrylate (PMMA), J. Fire Sci. 20 (2002), https://doi.org/10.1106/073490402027989.

[22] S. Lüftl, V.-M. Archodoulaki, S. Seidler, Thermal-oxidative induced degradation behaviour of polyoxymethylene (POM) copolymer detected by TGA/MS, Polym. Degrad. Stabil. 91 (2006) 464–471, https://doi.org/10.1016/j.polymdegradstab.2005.01.029.

[23] G. Berkowicz, T.M. Majka, W. Żukowski, The pyrolysis and combustion of polyoxymethylene in a fluidised bed with the possibility of incorporating CO2, Energy Convers. Manag. 214 (2020) 112888, https://doi.org/10.1016/j.enconman.2020.112888.

[24] I. Glassman, P. Yaccarino, The effect of oxygen concentration on sooting diffusion flames, Combust. Sci. Technol. 24 (1980) 107–114, https://doi.org/10.1080/00102208008952429.

[25] A. Tewarson, R.F. Pion, Flammability of plastics—I. Burning intensity, Combust. Flame 26 (1976) 85–103, https://doi.org/10.1016/0010-2180(76)90059-6.